LETTER

Molecular Structure Optimization of Fluorinated Ether Electrolyte for All Temperature Fast Charging Lithium-Ion Battery

Peiyuan Ma, Cindy Xue, Ke-Hsin Wang, Priyadarshini Mirmira, Minh Canh Vu, Oscar Rivera, and Chibueze V. Amanchukwu*

Cite This: ACS Energy Lett. 2024, 9, 6144–6152
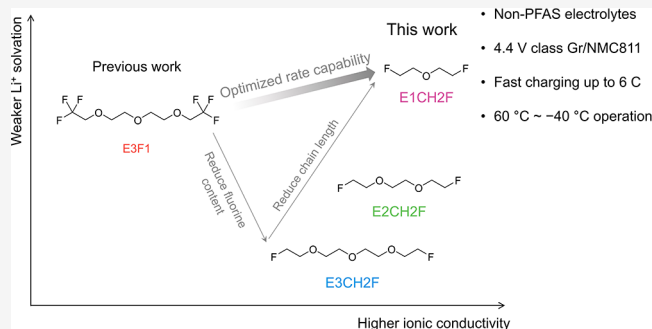
Read Online

ACCESS | Metrics & More | Article Recommendations | Supporting Information

ABSTRACT: New electrolytes are needed to replace commercial carbonate electrolytes to enable a wider working temperature range, higher energy density, and faster charging of lithium-ion batteries (LIBs). Fluorinated diluents and solvents have shown promise in LIB electrolyte design, but most of them are considered per- and polyfluoroalkyl substances (PFAS) with significant environmental and health concerns. In this work, we design a family of non-PFAS, partially fluorinated ether solvents for LIB electrolytes. Through rational molecular design, an optimized rate capability is achieved by low viscosity, weak lithium-ion solvation, and high ion diffusivity. The optimized electrolytes enable a longer cycle life and better rate capability

(up to 6 C) than previously reported fluorinated ethers or commercial carbonate electrolyte in graphite/LiNi$_{0.8}$Mn$_{0.1}$Co$_{0.1}$O$_2$ (Gr/NMC811) full cells. In addition, they also show an extended working temperature window with stable long-term cycling from 60 to −40 °C. This work shows a promising path to next generation batteries capable of extreme conditions without introducing PFAS concerns.

Lithium-ion batteries (LIBs) are state-of-the-art rechargeable batteries because they have high energy densities. As these batteries support newer applications, such as electric vehicles, even higher energy densities are needed as well as fast charging and a wider operating temperature window. While new anode (e.g., silicon) and cathode (e.g., high nickel) chemistries now exist with the promise of higher energy densities, deployment of new electrolytes has lagged.[1,2] Current LIBs are still reliant on electrolytes based on carbonate solvents such as ethylene carbonate (EC), linear carbonates, and a LiPF$_6$ salt. Unfortunately, the high melting point of EC and moderate thermal stability of LiPF$_6$ restrict the operation temperature window of carbonate electrolytes to −20 °C to +50 °C.[3] Carbonate solvents are also vulnerable to oxidative degradation and suffer from undesired transition metal dissolution with high voltage cathodes.[4,5] In addition, the strong lithium-ion binding to EC leads to a high desolvation energy barrier and sluggish charge transfer in carbonate electrolytes that may lead to undesired lithium metal plating under low temperature or

fast charging rate.[6−9] Therefore, newer approaches to electrolyte design are sorely needed.[10]
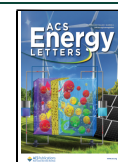
There has been a push in the literature to design "EC-free" electrolytes.[11] Hence, multiple solvent classes have been explored such as ethers, dimethyl sulfite or nitriles.[12−15] While those solvent classes show an extended working temperature window and enable faster charging, their compatibility with high voltage nickel-rich cathodes remains unclear. Our group revealed that fluorinated ether solvents can successfully suppress solvent co-intercalation and enable stable cycling of LIBs.[16] However, their rate capability, low temperature performance and oxidative stability remain to be studied and optimized.[16,17] Localized high concentration
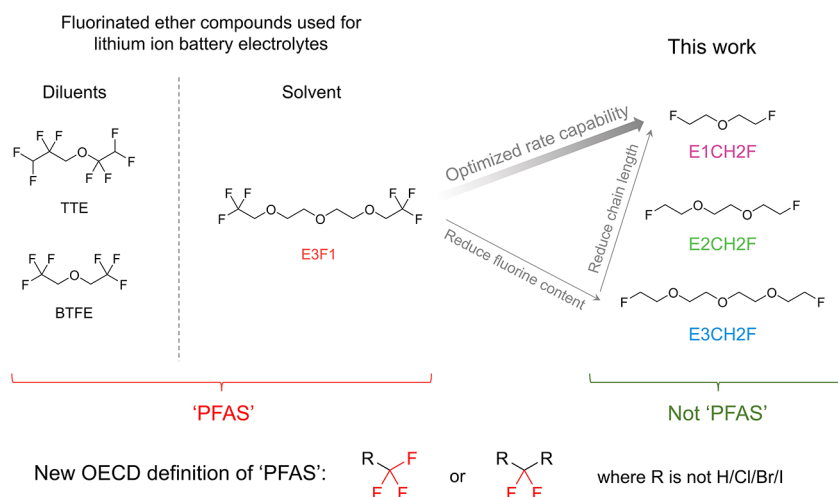
Figure 1. Molecular design strategy. Several fluorinated ether diluents and solvents have been reported for lithium-ion battery electrolytes but most of them are classified as potential per- and polyfluoroalkyl substances (PFAS) which are environmental hazards.[22,23] To improve the rate capability of fluorinated ether electrolytes and eliminate PFAS concerns, fluorine content is first reduced from previously reported E3F1 solvent to yield E3CH2F. By further reducing chain length, E1CH2F achieves optimized rate capability.

electrolytes (LHCE) with ether or carbonate solvents and fluorinated diluents can suppress solvent co-intercalation, enable fast charging and low temperature operation.[18−20] Recently, a combination of weakly solvating solvents and diluent enabled wide temperature operation, fast charging and compatibility with nickel-rich layered oxide cathode simultaneously.[21] However, the fluorinated diluents that are used in LHCEs may cause environmental concerns. According to the Organization for Economic Co-operation and Development (OECD), almost all the fluorinated diluents and solvents, such as bis(2,2,2-trifluoroethyl) ether (BTFE), 1,1,2,2-tetrafluoroethyl-2,2,3,3-tetrafluoropropyl ether (TTE) and E3F1,[16,17] may be classified as per- and polyfluoroalkyl substances (PFAS) (Figure 1).[22] PFAS are known to accumulate in the environment, are difficult to degrade, and are responsible for a wide range of health concerns.[23] Therefore, these electrolyte designs may not be commercialized even if they solve the technical problems that face LIB. This trend is witnessed by announcements of reducing or eliminating fluorinated compound production from companies such as 3M.[24]

In this work, we propose a partially fluorinated ether family (named the CH2F family) as non-PFAS electrolyte candidates for next-generation LIBs. The −CF$_3$ terminal group used in our previous work (E3F1[16,17]) is replaced with −CH$_2$F group to eliminate PFAS concerns. The molecular design of the CH2F family solvent is then systematically tuned to optimize the ion transport properties of the electrolyte (Figure 1). The optimized E1CH2F electrolyte not only outperforms previously reported fluorinated ether electrolytes in rate capability but also shows better cycling stability, higher rate capability (up to 6 C), and wider operation temperature window (60 to −40 °C) than commercial carbonate electrolyte in 4.4 V class graphite/LiNi$_{0.8}$Mn$_{0.1}$Co$_{0.1}$O$_2$ (Gr/NMC811) full cells. Our work shows a molecular design pathway to eliminating PFAS concerns and enabling next generation LIBs with high nickel content cathodes, wide working temperature range, and fast charging capability.

Rationale for Molecular Design and Synthesis. E3F1 studied in our previous work[17] has moderate ionic conductivity, which is due to high viscosity and strong ion pairing. Since strong ion pairing is believed to be beneficial for

facile interfacial kinetics[7,14] and electrochemical stability,[25−27] the main goal of the new molecular design is to decrease viscosity. Recent work on fluorinated ether solvent design for lithium metal battery have shown that further reducing glyme ether chain length of E3F1 results in insufficient solvation ability.[28] Therefore, we first replace the −CF$_3$ terminal group with the −CH$_2$F group to reduce fluorine content, which leads to a new family of fluorinated ether solvents named as the CH2F family. We then shrink the glyme ether chain within the CH2F family from E3CH2F to E1CH2F to achieve an even lower molecular weight. In the meantime, the CH2F family compounds are not considered as PFAS according to the new OECD definition because of the absence of perfluorinated groups. The CH2F family fluorinated ether solvents are synthesized by a one-step reaction between tetra-n-butylammonium fluoride (TBAF) and corresponding bis-tosylated ethylene glycols, as shown in Figure S1. The structure and product purity were verified using ^{1}H, ^{13}C, and ^{19}F nuclear magnetic resonance (NMR) spectroscopy (see the Supporting Information).

Ion Solvation Structure and Ion Transport. Ionic conductivity in the fluorinated ether electrolytes was probed using electrochemical impedance spectroscopy (EIS) and correlated to viscosity and ion solvation structure. Figure 2a shows the ionic conductivity of 1 M lithium bis(fluorosulfonyl)amide (LiFSA) in fluorinated ether solvents as a function of the temperature. At room temperature (20 °C), ionic conductivity increases in the order of E3F1 (0.93 mS/cm), E3CH2F (2.26 mS/cm), E2CH2F (5.36 mS/cm) and E1CH2F (5.74 mS/cm). The conductivities of the CH2F family electrolytes are greater than 1 mS/cm but still lower than those of carbonate electrolytes (10.5 mS/cm for ethylene carbonate/dimethyl carbonate 1 M LiPF$_6$). However, at temperatures below −30 °C, E1CH2F has higher conductivity than the carbonate electrolyte (1.44 mS/cm vs 0.49 mS/cm at −30 °C). As shown in Figure S2, E1CH2F also has the lowest activation energy barrier for ion transport. To understand the trend in conductivity, the viscosity of fluorinated ether solvents and electrolytes was measured (Figure 2b). Interestingly, E3CH2F has higher viscosity (5.08 mPa s) than E3F1 (2.62 mPa s) despite its lower molecular weight, which might be
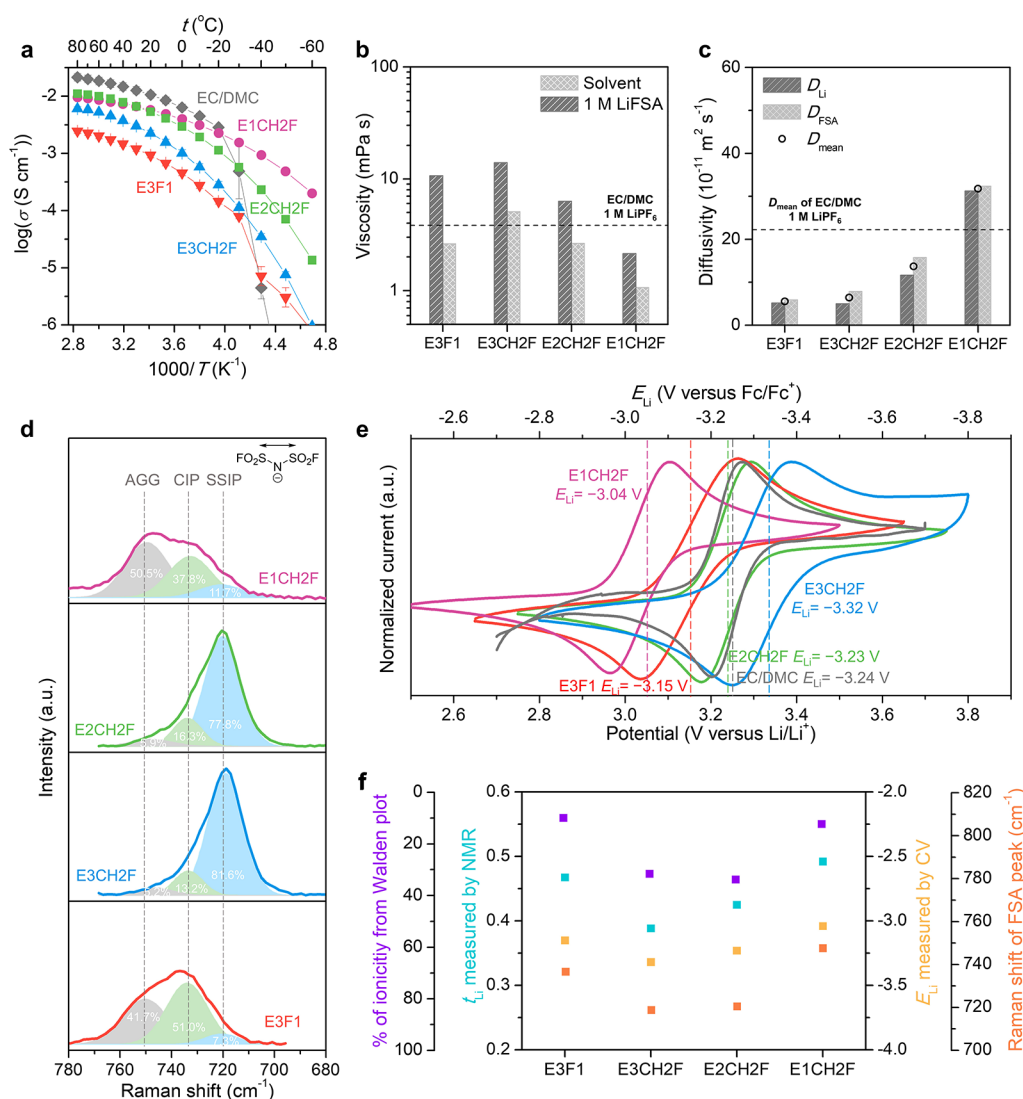
Figure 2. Ion transport and ion solvation. a) Ionic conductivity as a function of temperature of 1 M LiFSA in fluorinated ether electrolytes in comparison to 1 M LiPF$_6$ in EC/DMC (ethylene carbonate/dimethyl carbonate). The lines are to guide the eyes. **b)** Viscosity of fluorinated ether solvents and corresponding 1 M LiFSA electrolytes. **c)** Ion diffusivity of 1 M LiFSA in fluorinated ethers measured by PFG NMR. **d)** Raman peak of the FSA anion in 1 M LiFSA electrolytes. AGG: salt aggregates. CIP: contact-ion pair. SSIP: solvent-separated ion pair. The E3F1 data were extracted from ref 17. **e)** Lithium redox potential referenced to Fc/Fc$^+$ in 1 M LiFSA in fluorinated ether electrolytes in comparison to 1 M LiPF$_6$ in EC/DMC. **f)** Summary of ion transport indicators (percentage of ionicity from Walden plot and lithium transference number) and ion solvation indicators (E_{Li} and Raman shift of FSA peak), which shows the influence of the ion solvation structure on ion transport properties.

explained by increased polarity when replacing −CF$_3$ group with −CH$_2$F group.[29] From E3CH2F to E1CH2F, viscosity decreases with lower molecular weight and the E1CH2F electrolyte reaches the lowest viscosity of 2.15 mPa s, which is lower than the EC/DMC 1 M LiPF$_6$ electrolyte (3.85 mPa s). Ion diffusivity in fluorinated ether electrolytes was studied using pulsed-field gradient nuclear magnetic resonance (PFG NMR) spectroscopy. As Figure 2c shows, the ion diffusivity trend in general follows the Stokes−Einstein equation from E3CH2F to E1CH2F: less viscous electrolytes have higher ion diffusivity. However, the mean diffusivity (D_{mean}, defined as $(D_{Li}+D_{FSA})/2$) is higher despite increased viscosity from E3F1 (5.75×10^{-11} m^2/s) to E3CH2F (6.41×10^{-11} m^2/s), which might be due to less ion pairing in the E3CH2F electrolyte as discussed later. The least viscous electrolyte, E1CH2F 1 M LiFSA, has the highest D_{mean} of 31.83×10^{-11} m^2/s, which is

higher than EC/DMC 1 M LiPF$_6$ electrolyte ($D_{mean} = 22.19 \times 10^{-11}$ m^2/s).

While the ionic conductivity trend from E3CH2F to E1CH2F can be explained by decreasing viscosity, the Walden plot shown in Figure S3 indicates that ionic conductivity in fluorinated ether electrolytes is also strongly affected by ion dissociation or ion solvation structure. As shown in Figure 2d, the Raman peak of the FSA anion in 1 M LiFSA solutions shifts to higher wavenumbers from E3CH2F to E2CH2F to E3F1 to E1CH2F, indicating an increase in ion pairing. The deconvolution of Raman peak shows that E1CH2F leads to the highest fraction of salt aggregates (AGG) of 50.5%, while E2CH2F and E3CH2F electrolytes have a very high fraction of solvent separated ion pair (SSIP) of about 80%.[26] Figure 2e shows cyclic voltammetry (CV) curves of 1 M LiFSA in fluorinated ether electrolytes containing 1 mM ferrocene (Fc) in lithium/platinum (Li/Pt) cell, following the protocol
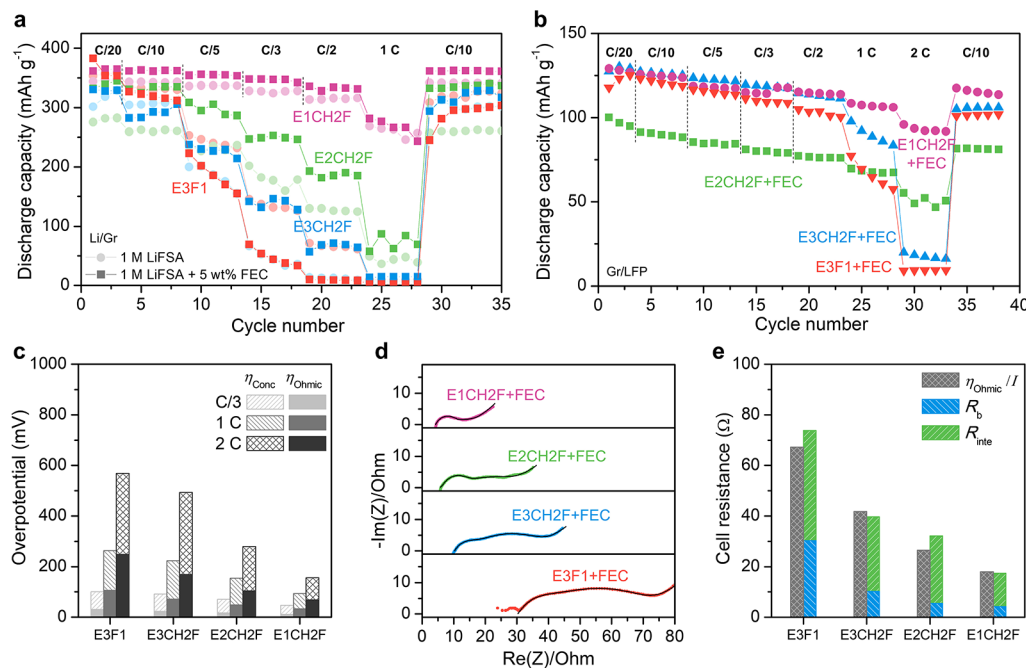
Figure 3. Rate capability. a) Rate capability test in Li/Gr cells. 1 C ≈ 2.17 mA/cm². b) Rate capability test in Gr/LFP cells using 1 M LiFSA electrolytes with 5 wt % FEC. 1 C ≈ 1.77 mA/cm². c) Breakdown of overpotential in Gr/LFP cells using 1 M LiFSA electrolytes with 5 wt % FEC. η_{Ohmic}: ohmic overpotential. η_{Conc}: concentration overpotential. d) EIS curve of Gr/LFP cells using 1 M LiFSA electrolytes with 5 wt % FEC. Solid lines indicate fitting curves. e) Comparison of Gr/LFP cell resistance calculated from overpotential (η_{Ohmic}/I) and resistance obtained from EIS. R_b: bulk resistance. R_{inte}: interfacial resistance.

recently reported by Yamada et al.[30] In the order E1CH2F, E3F1, E2CH2F and E3CH2F, decreasing E_{Li} (more reductive potentials) indicates stronger Li⁺ solvation environment and less ion pairing. Both Raman spectra and E_{Li} results suggest E1CH2F leads to strong ion pairing, similar to E3F1 and other reported fluorinated ether electrolytes,[31,32] while E2CH2F and E3CH2F have solvation structures closer to nonfluorinated glyme ethers or carbonate electrolytes.[33−35] The lower fraction of ion pairing in E3CH2F and E2CH2F can be explained by lower steric hindrance and stronger coordination ability of −CH₂F group as compared to the −CF₃ group in E3F1.[29,36]

Figure 2f summarizes four descriptors of the ion solvation environment from different techniques. The percentage of ionicity is calculated from the Walden plot shown in Figure S3. As an empirical rule, deviation from the diagonal KCl line (representing a fully dissociated electrolyte) in the Walden plot suggests the degree of ion dissociation in each nonideal electrolyte.[37] The lithium transference number is calculated as $t_{Li} = D_{Li}/(D_{Li} + D_{FSA})$ from ion diffusivity measured by PFG NMR, and more ion pairing leads to t_{Li} closer to 0.5. Raman shifts of the FSA peak and E_{Li} measured by CV are compared as a direct measure of ion solvation structure. The good correlation between indicators from ion transport (% of ionicity and t_{Li}) and direct indicators of ion solvation structure (Raman shifts of FSA peak and E_{Li}) suggests that the trend of ion transport properties can be explained by a combination of viscosity and solvation structure effects.

Correlating Rate Capability to Ion Transport. The rate capability of fluorinated ether electrolytes was tested in lithium/graphite (Li/Gr) half cells and graphite/LiFePO₄ (Gr/LFP) full cells. As discussed in supplementary note 1, fluoroethylene carbonate (FEC) was added to facilitate passivation and promote first cycle Coulombic efficiency. Figure 3a shows that the rate capability trend in the Li/Gr cell

follows E1CH2F > E2CH2F > E3F1 ≈ E3CH2F regardless of the addition of FEC. Figure 3b shows that the rate capability trend in the Gr/LFP cell agrees well with that of the Li/Gr cell, where E1CH2F electrolyte achieves the best rate capability by maintaining more than 80% of C/10 capacity at 2 C, similar to commercial carbonate electrolytes (Figure S9).

To understand the rate capability trend, the overpotential in Gr/LFP cells was measured by the galvanostatic intermittent titration technique (GITT).[38] As illustrated in Figures S10 and S11, cell overpotential can be divided into ohmic overpotential (η_{Ohmic}) and concentration overpotential(η_{Conc}). Among the fluorinated ether electrolytes, Figure 3c shows that total overpotential decreases from E3F1 to E3CH2F, E2CH2F, and E1CH2F, which agrees with the rate capability trend. Both η_{Ohmic} and η_{Conc} have significant contributions to the total overpotential, and they in general follow the same trend.

The trend in η_{Ohmic} has a clear correlation to cell resistance. Figure 3d shows the EIS curves of the Gr/LFP cells. Through fitting EIS curves with an equivalent circuit shown in Figure S12, cell resistance can be broken down into bulk resistance (R_b) and interfacial resistance (R_{inte}). Figure 3e shows that the total cell resistance obtained from EIS correlates well with cell resistance calculated from overpotential (η_{Ohmic} divided by current) and both R_b and R_{inte} decrease in the order E3F1, E3CH2F, E2CH2F, and E1CH2F. The decreasing trend of R_b from E3F1 to E1CH2F correlates well with their increasing ionic conductivity, which indicates the difference in R_b is mainly determined by electrolyte conductivity. Interfacial resistance arises from a series of interfacial processes including lithium-ion desolvation at the electrolyte/SEI interface, lithium-ion transport through SEI, and charge transfer at the SEI/electrode interface.[7,9] As discussed previously, the decreasing solvation power can explain the lowering of R_{inte} from E3CH2F to E1CH2F while the unexpectedly high R_{inte} in
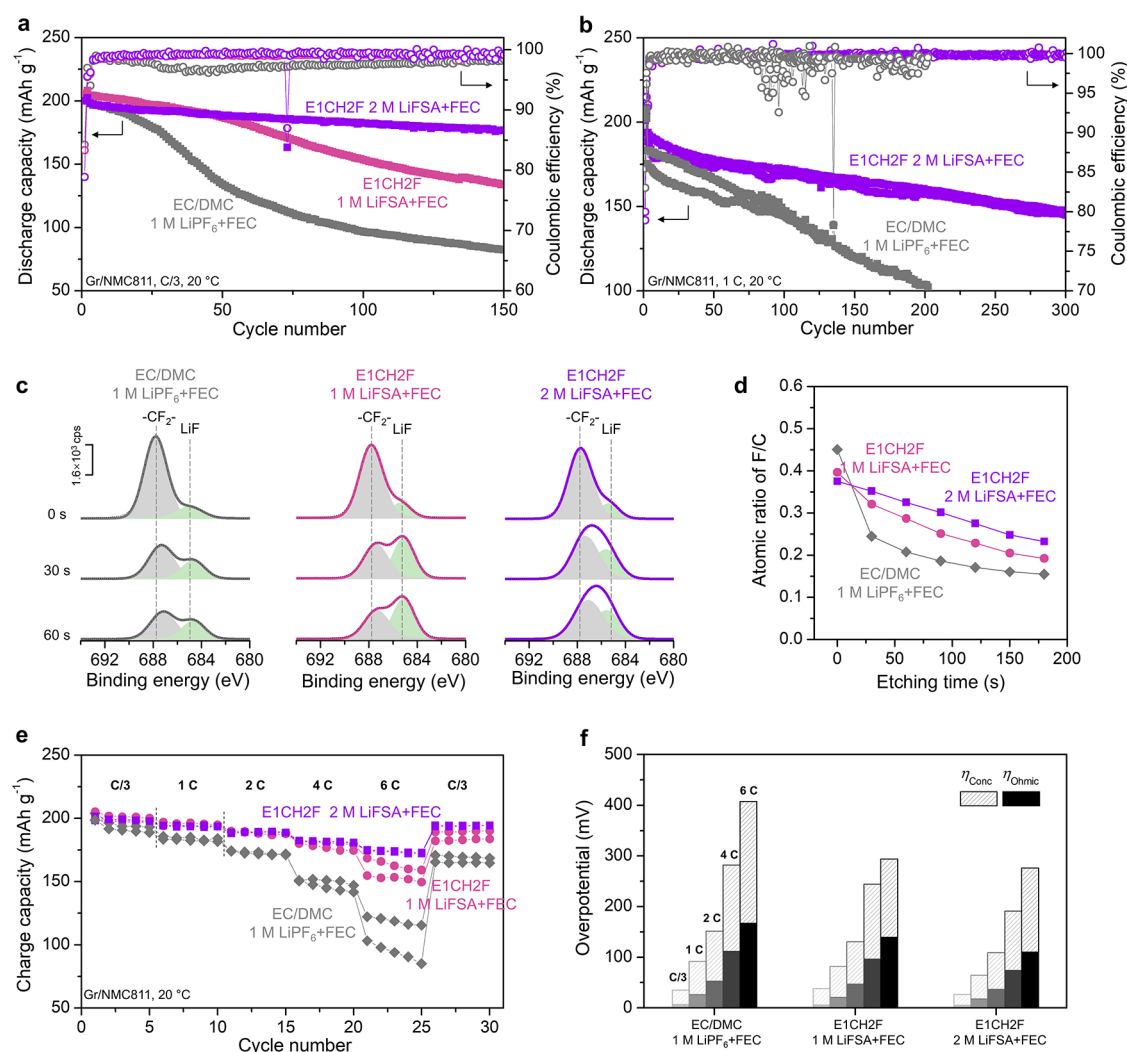
Figure 4. Gr/NMC811 full cell performance at room temperature. a) Cycling performance of Gr/NMC811 cells at a current rate of C/3. b) Cycling performance of Gr/NMC811 cells at a current rate of 1 C. Replicated cells are shown. c) F 1s XPS spectra of the NMC811 cathode after 100 cycles in corresponding electrolytes (ending on discharge). d) Atomic ratio between fluorine and carbon in the CEI of the NMC811 electrode as a function of sputtering time. e) Fast charging test of Gr/NMC811 cells at varying charging current rates up to 6 C and a constant discharging current rate of C/3. Replicated cells are shown. f) Breakdown of overpotential in Gr/NMC811 cells as a function of electrolyte and current rate. η_{Ohmic}: ohmic overpotential. η_{Conc}: concentration overpotential. 1 C ≈ 1.66 mA/cm^2 for Gr/NMC811 cells.

E3F1 electrolyte might originate from its thick and resistive SEI.[16]

By definition, η_{Conc} originates from the concentration gradient built with polarization.[39] While theories are developed to describe the concentration gradient and simulate η_{Conc}, they are complicated and require multiple parameters that are not easily accessible.[40] In addition, unlike η_{Ohmic}, η_{Conc} shows dependence on the state of the charge (Figure S11), indicating the contribution from electrode materials. Therefore, we utilize only a simplified model to illustrate qualitatively. As discussed in supplementary note 2, after simplification, the strength of concentration gradient can be correlated to lithium diffusivity: concentration gradient $\propto 1/D_{Li}$. Since D_{Li} follows the trend E3F1 ≈ E3CH2F < E2CH2F < E1CH2F, the strength of concentration gradient and η_{Conc} decrease in the order E3F1 ≈ E3CH2F > E2CH2F > E1CH2F. In summary, rate capability is influenced by multiple factors and E1CH2F shows good rate capability because of its high ionic conductivity, weak lithium ion solvation, and high lithium ion diffusivity.

Performance in Gr/NMC811 Full Cell under Extreme Conditions. The promise of E1CH2F electrolyte in commercial lithium-ion battery configuration is illustrated by full cell cycling using the Ni-rich NMC811 cathode. Figure 4a shows the cycling performance of the Gr/NMC811 full cell at a current rate of C/3 at 20 °C (1 C ≈ 1.66 mA/cm^2, n/p ≈ 1.3). Compared to the carbonate electrolyte control (EC/DMC 1 M LiPF$_6$ + 5 wt % FEC), E1CH2F electrolyte (1 M) has better capacity retention and higher Coulombic efficiency. With higher salt concentration, E1CH2F 2 M LiFSA + 5 wt % FEC electrolyte enables further improved cycling stability with 89% capacity retention at the 150th cycle. E1CH2F electrolyte also maintains superior capacity retention than carbonate electrolyte control in 1 C cycling of Gr/NMC811 cells, as shown in Figure 4b (76% at 300th cycle vs 56% at 200th cycle). As shown in Figure 4c,d and Figure S13, X-ray photoelectron spectroscopy (XPS) reveals that E1CH2F electrolytes show a higher content of LiF in the cathode electrolyte interphase (CEI) than carbonate electrolytes. As proposed in the literature, a higher content of inorganic
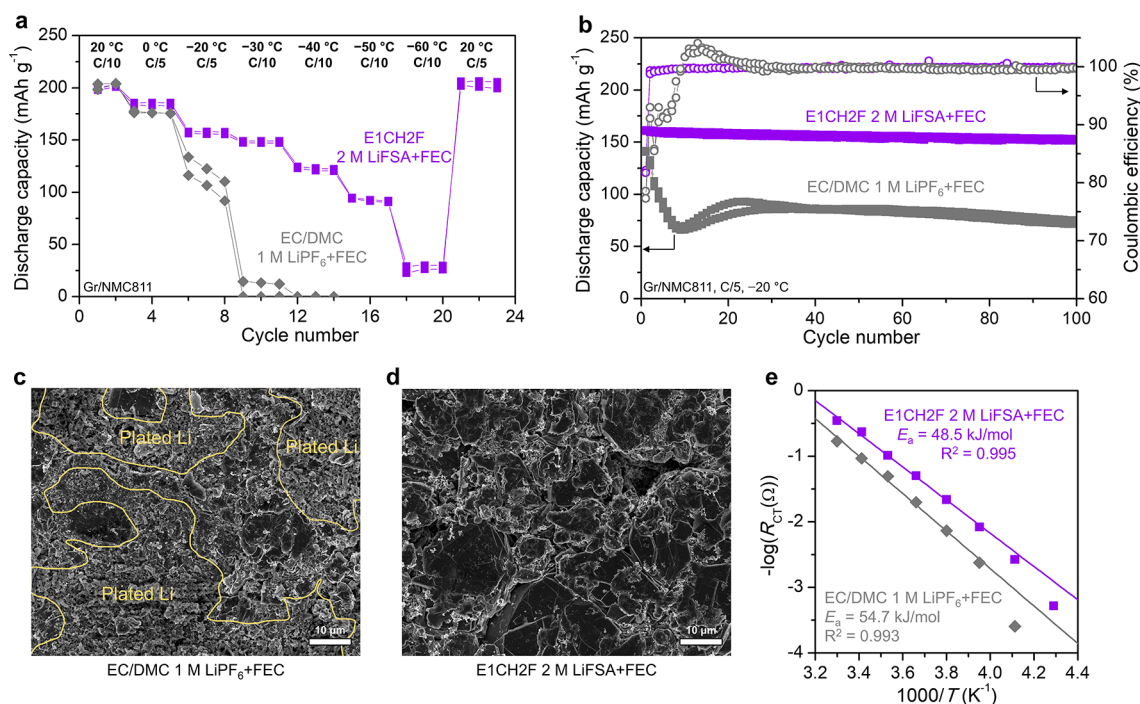
Figure 5. Gr/NMC811 full cell performance at low temperature. a) Cycling performance of Gr/NMC811 cells at temperatures varying from 20 to −60 °C. 1 C ≈ 1.66 mA/cm². b) Long-term cycling of Gr/NMC811 cells at −20 °C. c, d) SEM images of graphite electrode after 100 cycles in Gr/NMC811 cells at −20 °C (ending on discharge). e) Charge transfer resistance of Gr/NMC811 cells as a function of temperature. Straight lines represent linear fitting of data between 30 and −20 °C.

components such as LiF in CEI likely leads to better stability of the interfacial layer that helps to protect the NMC811 electrode from degradation.[41] Figure S14 shows cross section scanning electron microscope (SEM) images of the cycled NMC811 electrode, where cracking of NMC811 particles can be observed after cycling in carbonate electrolyte whereas little cracking is observed in the sample cycled in E1CH2F electrolytes. Figures S15 and S16 show that E1CH2F electrolytes have only slightly better oxidative stability than carbonate electrolyte in CV or the potentiostatic hold test. Hence, the better NMC811 cathode compatibility of E1CH2F electrolytes likely originates from the more robust CEI that protects NMC811 from degradation.

The rate capability of the E1CH2F electrolyte in the Gr/NMC811 full cell was also studied. As shown in Figure 4e, E1CH2F electrolytes support fast charging up to 6 C (~11 mA/cm²) while maintaining ~77% and ~85% of C/3 capacity for 1 and 2 M salt concentration, respectively. In contrast, the carbonate electrolyte can only maintain ~52% of C/3 capacity when charged at 6 C. Figure S17 shows that E1CH2F electrolytes also enable better long-term cycling stability than the carbonate electrolyte at a high current rate. Figure 4f shows that E1CH2F electrolytes have lower η_{Conc} and η_{Ohmic} than carbonate electrolyte in Gr/NMC811 cells, as measured by GITT. Following the same analysis in the previous section, the lower η_{Conc} of 1 M E1CH2F electrolyte can be attributed to its higher ion diffusivity and higher transference number compared to carbonate electrolyte (Figure S18). Although increasing salt concentration leads to slightly lower mean ion diffusivity in 2 M E1CH2F electrolyte, it maintains higher lithium transference number and lithium ion diffusivity than the carbonate electrolyte. Moreover, under a similar concentration gradient strength, the higher concentration itself should help to maintain lithium ion concentration at the anode and

reduce concentration overpotential during fast charging. Regarding η_{Ohmic}, the EIS test of Gr/NMC811 cells shown in Figure S19 reveals that the lower ohmic overpotential of E1CH2F electrolytes should be attributed to their lower interfacial resistance while the bulk resistance of E1CH2F and carbonate electrolytes are similar.

To investigate the working temperature range of the E1CH2F electrolytes, full cell cycling was performed at variable temperatures. Figure S20 shows the cycling of Gr/NMC811 cells at 60 °C. Despite slightly faster capacity decay than room temperature, E1CH2F 2 M LiFSA + FEC electrolyte can be cycled stably at 60 °C and maintain an average discharge capacity of 149.4 mAh/g after 150 cycles, which is ~91% of its capacity at 20 °C in the same cycle number. The low temperature performance of E1CH2F electrolyte was first tested at temperatures ranging from 20 to −60 °C. As shown in Figure 5a, the E1CH2F electrolyte can deliver 46% of room temperature capacity at −50 °C and can fully recover its room temperature capacity after short-term cycling at −60 °C, which demonstrates its tolerance to extreme low temperature. By contrast, the carbonate electrolyte shows significant capacity decay at −20 °C and can barely cycle below −30 °C, in accordance to literature reports.[14,15,21] As shown in Figure S21, the conductivity of carbonate electrolytes drops rapidly below −30 °C due to phase transition while E1CH2F electrolytes maintain relatively high ionic conductivity at low temperatures without obvious phase change (confirmed by DSC shown in Figure S22). As shown in Figure 5b, the E1CH2F electrolyte enables stable long-term cycling at −20 °C with 94% capacity retention in 100 cycles, while the carbonate electrolyte has unstable cycling profiles. Figure S23 shows that E1CH2F electrolyte can also enable long-term stable cycling up to −40 °C. As shown in Figure 5c and Figure S24, SEM and energy-dispersive X-ray spectroscopy

(EDS) mapping indicate that carbonate electrolyte leads to significant lithium plating on graphite during −20 °C cycling.[8,42] In contrast, Figure 5d and Figure S25 show that no obvious lithium plating is observed on graphite electrodes cycled in the E1CH2F electrolyte at −20 °C. To further understand low temperature performance, EIS was performed on Gr/NMC811 cells at low temperatures. As shown in Figure S26, the cell resistance at low temperature is dominated by charge transfer resistance (R_{CT}). Compared to the carbonate electrolyte, Figure 5e shows that the E1CH2F electrolyte has a lower R_{CT} and lower activation energy of charge transfer, which likely leads to better intercalation kinetics at low temperatures and helps to avoid lithium plating.

In this work, we report the molecular structure optimization of fluorinated ether solvents for lithium ion batteries. With a −CH2F end group and short glyme ether chain length, E1CH2F achieves lower viscosity while maintaining weak lithium-ion solvation and also eliminating PFAS concerns. The poorer reduction stability of CH2F family electrolytes causes sluggish passivation of the graphite electrode, necessitating the introduction of 5 wt % FEC additive to improve first cycle Coulombic efficiency. Due to higher ionic conductivity, higher lithium-ion diffusivity, and lower interfacial resistance, E1CH2F electrolyte leads to improved rate capability compared to other fluorinated ethers. Furthermore, E1CH2F electrolytes show better capacity retention than carbonate electrolyte in Gr/NMC811 full cells due to the formation of a LiF-rich CEI that preserves the NMC811 electrode from degradation. They also show better rate capability than carbonate electrolytes, owing to their higher lithium-ion diffusivity and lower interfacial resistance. Finally, at low temperatures, E1CH2F electrolytes can tolerate −60 °C operation and support −40 °C stable cycling of the Gr/NMC811 cells. Our molecular design strategy opens a new route of fluorinated electrolyte development for wide working temperature, high voltage, and fast charging batteries with fewer environmental concerns.

ASSOCIATED CONTENT

Supporting Information

The Supporting Information is available free of charge at https://pubs.acs.org/doi/10.1021/acsenergylett.4c01999.

Experimental section, figures and notes including Li intercalation mechanism, Derivation of concentration gradient; properties of solvents, electrode specifications, synthetic scheme, Fitting of conductivity-temperature data, Walden plot, electrochemical data, XRD, NMR, XPS, and EDS spectra, DFT calculation data, EIS data, GITT data, SEM images, DSC data and battery cycling data (PDF)

AUTHOR INFORMATION

Corresponding Author

Chibueze V. Amanchukwu − *Pritzker School of Molecular Engineering, University of Chicago, Chicago, Illinois 60637, United States;* orcid.org/0000-0002-6573-1213; Email: chibueze@uchicago.edu

Authors

Peiyuan Ma − *Pritzker School of Molecular Engineering, University of Chicago, Chicago, Illinois 60637, United States*

Cindy Xue − *Pritzker School of Molecular Engineering, University of Chicago, Chicago, Illinois 60637, United States*

Ke-Hsin Wang − *Pritzker School of Molecular Engineering, University of Chicago, Chicago, Illinois 60637, United States;* orcid.org/0009-0003-0263-2546

Priyadarshini Mirmira − *Pritzker School of Molecular Engineering, University of Chicago, Chicago, Illinois 60637, United States;* orcid.org/0000-0002-3004-7227

Minh Canh Vu − *Pritzker School of Molecular Engineering, University of Chicago, Chicago, Illinois 60637, United States*

Oscar Rivera − *Pritzker School of Molecular Engineering, University of Chicago, Chicago, Illinois 60637, United States*

Complete contact information is available at:
https://pubs.acs.org/10.1021/acsenergylett.4c01999

Notes

The authors declare no competing financial interest.

REFERENCES

(1) Winter, M.; Barnett, B.; Xu, K. Before Li Ion Batteries. *Chem. Rev.* **2018**, *118* (23), 11433−11456.

(2) Meng, Y. S.; Srinivasan, V.; Xu, K. Designing Better Electrolytes. *Science* **2022**, *378* (6624), No. eabq3750.

(3) Xu, K. Nonaqueous Liquid Electrolytes for Lithium-Based Rechargeable Batteries. *Chem. Rev.* **2004**, *104* (10), 4303−4418.

(4) Klein, S.; van Wickeren, S.; Röser, S.; Bärmann, P.; Borzutzki, K.; Heidrich, B.; Börner, M.; Winter, M.; Placke, T.; Kasnatscheew, J. Understanding the Outstanding High-Voltage Performance of NCM523‖Graphite Lithium Ion Cells after Elimination of Ethylene Carbonate Solvent from Conventional Electrolyte. *Adv. Energy Mater.* **2021**, *11* (14), 2003738.

(5) Ruff, Z.; Xu, C.; Grey, C. P. Transition Metal Dissolution and Degradation in NMC811-Graphite Electrochemical Cells. *J. Electrochem. Soc.* **2021**, *168* (6), 060518.

(6) Zhang, S. S.; Xu, K.; Jow, T. R. A New Approach toward Improved Low Temperature Performance of Li-Ion Battery. *Electrochem. commun.* **2002**, *4* (11), 928−932.

(7) Lee, H.; An, H.; Chang, H.; Lee, M.; Park, S.; Lee, S.; Kang, J.; Byon, S.; Koo, B.; Lee, H.; Lee, Y. M.; Moon, J.; Chae, S.; Lee, H. Boosting Interfacial Kinetics in Extremely Fast Rechargeable Li-Ion

Batteries with Linear Carbonate-Based, LiPF6-Concentrated Electrolyte. *Energy Storage Mater.* **2023**, *63*, 102995.

(8) Petzl, M.; Kasper, M.; Danzer, M. A. Lithium Plating in a Commercial Lithium-Ion Battery - A Low-Temperature Aging Study. *J. Power Sources* **2015**, *275*, 799−807.

(9) Hu, A.; Li, F.; Chen, W.; Lei, T.; Li, Y.; Fan, Y.; He, M.; Wang, F.; Zhou, M.; Hu, Y.; Yan, Y.; Chen, B.; Zhu, J.; Long, J.; Wang, X.; Xiong, J. Ion Transport Kinetics in Low-Temperature Lithium Metal Batteries. *Adv. Energy Mater.* **2022**, *12* (42), 2202432.

(10) Amanchukwu, C. V. The Electrolyte Frontier: A Manifesto. *Joule* **2020**, *4* (2), 281−285.

(11) Pan, R.; Cui, Z.; Yi, M.; Xie, Q.; Manthiram, A. Ethylene Carbonate-Free Electrolytes for Stable, Safer High-Nickel Lithium-Ion Batteries. *Adv. Energy Mater.* **2022**, *12* (19), 2103806.

(12) Zhao, Y.; Hu, Z.; Zhao, Z.; Chen, X.; Zhang, S.; Gao, J.; Luo, J. Strong Solvent and Dual Lithium Salts Enable Fast-Charging Lithium-Ion Batteries Operating from −78 to 60 °C. *J. Am. Chem. Soc.* **2023**, *145* (40), 22184−22193.

(13) Luo, L.; Chen, K.; Chen, H.; Li, H.; Cao, R.; Feng, X.; Chen, W.; Fang, Y.; Cao, Y. Enabling Ultralow-Temperature (−70 °C) Lithium-Ion Batteries: Advanced Electrolytes Utilizing Weak-Solvation and Low-Viscosity Nitrile Cosolvent. *Adv. Mater.* **2024**, *36* (5), 2308881.

(14) Xia, D.; Kamphaus, E. P.; Hu, A.; Hwang, S.; Tao, L.; Sainio, S.; Nordlund, D.; Fu, Y.; Huang, H.; Cheng, L.; Lin, F. Design Criteria of Dilute Ether Electrolytes toward Reversible and Fast Intercalation Chemistry of Graphite Anode in Li-Ion Batteries. *ACS Energy Lett.* **2023**, *8* (3), 1379−1389.

(15) Wang, Z.; Han, R.; Huang, D.; Wei, Y.; Song, H.; Liu, Y.; Xue, J.; Zhang, H.; Zhang, F.; Liu, L.; Weng, S.; Lu, S.; Xu, J.; Wu, X.; Wei, Z. Co-Intercalation-Free Ether-Based Weakly Solvating Electrolytes Enable Fast-Charging and Wide-Temperature Lithium-Ion Batteries. *ACS Nano* **2023**, *17* (18), 18103−18113.

(16) Ma, P.; Mirmira, P.; Eng, P. J.; Son, S.-B.; Bloom, I. D.; Filatov, A. S.; Amanchukwu, C. V. Co-Intercalation-Free Ether Electrolytes for Graphitic Anodes in Lithium-Ion Batteries. *Energy Environ. Sci.* **2022**, *15* (11), 4823−4835.

(17) Ma, P.; Mirmira, P.; Amanchukwu, C. V. Effect of Building Block Connectivity and Ion Solvation on Electrochemical Stability and Ionic Conductivity in Novel Fluoroether Electrolytes. *ACS Cent. Sci.* **2021**, *7* (7), 1232−1244.

(18) Zhang, X.; Zou, L.; Xu, Y.; Cao, X.; Engelhard, M. H.; Matthews, B. E.; Zhong, L.; Wu, H.; Jia, H.; Ren, X.; Gao, P.; Chen, Z.; Qin, Y.; Kompella, C.; Arey, B. W.; Li, J.; Wang, D.; Wang, C.; Zhang, J.-G.; Xu, W. Advanced Electrolytes for Fast-Charging High-Voltage Lithium-Ion Batteries in Wide-Temperature Range. *Adv. Energy Mater.* **2020**, *10* (22), 2000368.

(19) Jia, H.; Xu, Y.; Burton, S. D.; Gao, P.; Zhang, X.; Matthews, B. E.; Engelhard, M. H.; Zhong, L.; Bowden, M. E.; Xiao, B.; Han, K. S.; Wang, C.; Xu, W. Enabling Ether-Based Electrolytes for Long Cycle Life of Lithium-Ion Batteries at High Charge Voltage. *ACS Appl. Mater. Interfaces* **2020**, *12* (49), 54893−54903.

(20) Jiang, L.-L.; Yan, C.; Yao, Y.-X.; Cai, W.; Huang, J.-Q.; Zhang, Q. Inhibiting Solvent Co-Intercalation in a Graphite Anode by a Localized High-Concentration Electrolyte in Fast-Charging Batteries. *Angew. Chemie Int. Ed.* **2021**, *60* (7), 3402−3406.

(21) Xu, J.; Zhang, J.; Pollard, T. P.; Li, Q.; Tan, S.; Hou, S.; Wan, H.; Chen, F.; He, H.; Hu, E.; Xu, K.; Yang, X.-Q.; Borodin, O.; Wang, C. Electrolyte Design for Li-Ion Batteries under Extreme Operating Conditions. *Nature* **2023**, *614* (7949), 694−700.

(22) Wang, Z.; Buser, A. M.; Cousins, I. T.; Demattio, S.; Drost, W.; Johansson, O.; Ohno, K.; Patlewicz, G.; Richard, A. M.; Walker, G. W.; White, G. S.; Leinala, E. A New OECD Definition for Per- and Polyfluoroalkyl Substances. *Environ. Sci. Technol.* **2021**, *55* (23), 15575−15578.

(23) Evich, M. G.; Davis, M. J. B.; McCord, J. P.; Acrey, B.; Awkerman, J. A.; Knappe, D. R. U.; Lindstrom, A. B.; Speth, T. F.; Tebes-Stevens, C.; Strynar, M. J.; Wang, Z.; Weber, E. J.; Henderson, W. M.; Washington, J. W. Per- and Polyfluoroalkyl Substances in the Environment. *Science (80-.).* **2022**, *375* (6580), No. eabg9065.

(24) 3M. 3M to Exit PFAS Manufacturing by the End of 2025. https://news.3m.com/2022-12-20-3M-to-Exit-PFAS-Manufacturing-by-the-End-of-2025 (accessed June 17, 2024).

(25) Yamada, Y.; Furukawa, K.; Sodeyama, K.; Kikuchi, K.; Yaegashi, M.; Tateyama, Y.; Yamada, A. Unusual Stability of Acetonitrile-Based Superconcentrated Electrolytes for Fast-Charging Lithium-Ion Batteries. *J. Am. Chem. Soc.* **2014**, *136* (13), 5039−5046.

(26) Wang, J.; Yamada, Y.; Sodeyama, K.; Chiang, C. H.; Tateyama, Y.; Yamada, A. Superconcentrated Electrolytes for a High-Voltage Lithium-Ion Battery. *Nat. Commun.* **2016**, *7* (1), 12032.

(27) Fan, X.; Chen, L.; Ji, X.; Deng, T.; Hou, S.; Chen, J.; Zheng, J.; Wang, F.; Jiang, J.; Xu, K.; Wang, C. Highly Fluorinated Interphases Enable High-Voltage Li-Metal Batteries. *Chem.* **2018**, *4* (1), 174−185.

(28) Yu, Z.; Rudnicki, P. E.; Zhang, Z.; Huang, Z.; Celik, H.; Oyakhire, S. T.; Chen, Y.; Kong, X.; Kim, S. C.; Xiao, X.; Wang, H.; Zheng, Y.; Kamat, G. A.; Kim, M. S.; Bent, S. F.; Qin, J.; Cui, Y.; Bao, Z. Rational Solvent Molecule Tuning for High-Performance Lithium Metal Battery Electrolytes. *Nat. Energy* **2022**, *7* (1), 94−106.

(29) Yu, Z.; Yu, W.; Chen, Y.; Mondonico, L.; Xiao, X.; Zheng, Y.; Liu, F.; Hung, S. T.; Cui, Y.; Bao, Z. Tuning Fluorination of Linear Carbonate for Lithium-Ion Batteries. *J. Electrochem. Soc.* **2022**, *169* (4), 040555.

(30) Ko, S.; Obukata, T.; Shimada, T.; Takenaka, N.; Nakayama, M.; Yamada, A.; Yamada, Y. Electrode Potential Influences the Reversibility of Lithium-Metal Anodes. *Nat. Energy* **2022**, *7*, 1217−1224.

(31) Zhao, Y.; Zhou, T.; Ashirov, T.; Kazzi, M. El; Cancellieri, C.; Jeurgens, L. P. H.; Choi, J. W.; Coskun, A. Fluorinated Ether Electrolyte with Controlled Solvation Structure for High Voltage Lithium Metal Batteries. *Nat. Commun.* **2022**, *13* (1), 2575.

(32) Zhou, T.; Zhao, Y.; El Kazzi, M.; Choi, J. W.; Coskun, A. Integrated Ring-Chain Design of a New Fluorinated Ether Solvent for High-Voltage Lithium-Metal Batteries. *Angew. Chemie Int. Ed.* **2022**, *61*, No. e202115884.

(33) Zhang, P.; Jin, H.; Wang, T.; Wang, M. Insight into the Effect of Lithium-Dendrite Suppression by Lithium Bis(Fluorosulfony)-Imide/1,2-Dimethoxyethane Electrolytes. *Electrochim. Acta* **2018**, *277*, 116−126.

(34) Koo, B.; Lee, H.; Hwang, S.; Lee, J.; Han, Y.-K.; Ahn, K. H.; Lee, C.; Lee, H. Role of Solvent Isomerism in Mixed Carbonate Electrolytes for Li-Ion Batteries. *J. Phys. Chem. C* **2023**, *127* (37), 18271−18278.

(35) Seo, D. M.; Reininger, S.; Kutcher, M.; Redmond, K.; Euler, W. B.; Lucht, B. L. Role of Mixed Solvation and Ion Pairing in the Solution Structure of Lithium Ion Battery Electrolytes. *J. Phys. Chem. C* **2015**, *119* (25), 14038−14046.

(36) Ma, P.; Kumar, R.; Vu, M. C.; Wang, K.-H.; Mirmira, P.; Amanchukwu, C. V. Fluorination Promotes Lithium Salt Dissolution in Borate Esters for Lithium Metal Batteries. *J. Mater. Chem. A* **2024**, *12* (4), 2479−2490.

(37) Wang, Y.; Chen, W.; Zhao, Q.; Jin, G.; Xue, Z.; Wang, Y.; Mu, T. Ionicity of Deep Eutectic Solvents by Walden Plot and Pulsed Field Gradient Nuclear Magnetic Resonance (PFG-NMR). *Phys. Chem. Chem. Phys.* **2020**, *22* (44), 25760−25768.

(38) Kim, J.; Park, S.; Hwang, S.; Yoon, W.-S. Principles and Applications of Galvanostatic Intermittent Titration Technique for Lithium-Ion Batteries. *J. Electrochem. Sci. Technol.* **2022**, *13* (1), 19−31.

(39) Fuller, T. F.; Harb, J. N. *Electrochemical Engineering*; Wiley: Hoboken, 2018.

(40) Wang, A. A.; Gunnarsdóttir, A. B.; Fawdon, J.; Pasta, M.; Grey, C. P.; Monroe, C. W. Potentiometric MRI of a Superconcentrated Lithium Electrolyte: Testing the Irreversible Thermodynamics Approach. *ACS Energy Lett.* **2021**, *6* (9), 3086−3095.

(41) Xue, W.; Huang, M.; Li, Y.; Zhu, Y. G.; Gao, R.; Xiao, X.; Zhang, W.; Li, S.; Xu, G.; Yu, Y.; Li, P.; Lopez, J.; Yu, D.; Dong, Y.; Fan, W.; Shi, Z.; Xiong, R.; Sun, C. J.; Hwang, I.; Lee, W. K.; Shao-

Horn, Y.; Johnson, J. A.; Li, J. Ultra-High-Voltage Ni-Rich Layered Cathodes in Practical Li Metal Batteries Enabled by a Sulfonamide-Based Electrolyte. *Nat. Energy* **2021**, *6* (5), 495−505.

(42) Ng, B.; Coman, P. T.; Faegh, E.; Peng, X.; Karakalos, S. G.; Jin, X.; Mustain, W. E.; White, R. E. Low-Temperature Lithium Plating/Corrosion Hazard in Lithium-Ion Batteries: Electrode Rippling, Variable States of Charge, and Thermal and Nonthermal Runaway. *ACS Appl. Energy Mater.* **2020**, *3* (4), 3653−3664.